Five-Degree-of-Freedom Magnetic Control of Micro-Robots Using Rotating Permanent Magnets

Patrick Ryan and Eric Diller

Abstract— **Recent work in magnetically-actuated micro-scale robots for biomedical or microfluidic applications has resulted in electromagnetic actuation systems which can command precise five degree of freedom control of simple magnetic devices at the sub-millimeter scale. This paper presents a simple actuation system which uses an array of large, rotatable permanent magnets to generate the same level of control over untethered micro-robotic systems. We show that the system can generate any field or field gradient at the workspace (including a value of zero). In contrast with previous permanent magnet actuation systems, the system proposed here accomplishes this without any hazardous translational motion of the control magnets, resulting in a simple, safe, and inexpensive system. The system exhibits similar capabilities to electromagnetic actuation systems, with potential for stronger field production and minimal heat generation. The prototype system presented, with eight permanent magnets, can create fields and gradients in any direction with strength of 30 mT and 0.9 T·m^{-1}, respectively. The effectiveness of the system is shown through characterization and feedback control of a 250 μm micro-magnet in a proof-of-concept path-following task with average accuracy of 39 μm.**

I. Introduction

The wireless control of small devices is an exciting prospect due to the ability of these devices to access enclosed spaces such as those within the human body. The use of externally-generated magnetic fields has been shown to be a preferred method for control of untethered devices that range in size from micrometers to centimeters when physical tethers to the device are not possible. This type of magnetic control is suitable for operation of wireless devices in confined spaces, and therefore has many applications in the medical field including ophthalmic procedures [1], catheter steering [2], and wireless capsule endoscopy [3] as well as applications in micro-object manipulation including operations involving single cells [4], and microparticles [5]. The use of wireless magnetic devices will offer benefits over current surgical techniques by allowing an increased level of control, decreased device sizes and faster procedure completion.

For many applications involving wireless magnetic actuation, a high level of control of the position and orientation of the micro-device is required. An implement containing a single permanent magnet can be positioned with a maximum of five degrees of freedom (DOF), consisting of three translational DOF and two rotational DOF. Actuation systems that use electromagnetic coils to generate the magnetic fields have been shown to be capable of controlling a single magnetic device with 5 DOF [1],[6]. Three-dimensional control of multiple microrobots has also been demonstrated using similar electromagnet systems [7].

An alternative method for field generation is to use permanent magnets instead of electromagnetic coils. Both electromagnets and permanent magnets generate an equivalent magnetic field, however, the use of electromagnetics has often been the preferred technique due to the ability to control the field strength by changing the coil current. This enables high frequency field modulation, and the ability to turn off the field completely. Such electromagnet systems, however, are limited in that the high current required for strong field generation results in a significant temperature rise within the coils. The heating of coils often requires active cooling solutions, and can result in increased workplace temperature, making this type of system unsuitable for heat-sensitive applications such as biomedical applications involving cells. If permanent magnets are instead used as the field source, the field is produced using no input power resulting in no heat generation near the workspace. Additionally, relative to electromagnetic devices, permanent magnet systems are able to generate stronger fields and field gradients by a factor of approximately 10-20, and 2-3, respectively [8]. An increase in field magnitude results in faster motions for magnetic crawling [9],[10] and swimming robots [11] while an increase in field gradient magnitude yields stronger magnetic forces for gradient pulling.

Permanent magnet systems have been shown to be capable of providing 4 DOF control of a capsule endoscopes by using a hand-held [13] or robotically actuated [14],[15] permanent magnet positioned outside the body. The Stereotaxis Niobe system uses permanent magnets for catheter steering and is currently in clinical use [2]. Recently, a permanent magnet system has been shown to be capable of 5 DOF control of a capsule endoscope using a single permanent magnet positioned above the workspace using a robotic manipulator [3]. This method has demonstrated the highest level of control for a permanent magnet system but downsides are the potential hazard of the mobile robotic manipulator and the high cost of the system. The system shown in [16] uses an array of continuously rotating magnets, positioned symmetrically around the workspace for simple and safe field production, although this system is limited to producing only in-plane uniform rotating magnetic fields.

In this paper, we propose a new method to achieve full 5 DOF control using permanent magnets that rotate in place. Unlike the robotically-manipulated single magnet system mentioned above in [3], the proposed system is composed of multiple permanent magnets, each with the ability to be rotated about its own fixed axis, independently of the other magnets. We show that this system can be used to generate magnetic fields and gradients in any direction with strengths comparable or exceeding those of existing electromagnetic and permanent magnet systems. Each magnet rotates about its volumetric center, hence the system contains no translating components

Research supported by the Canadian Natural Sciences Engineering Research Council Discovery Grants Program and P. Ryan is supported by the NSERC CGS-M fellowship.

P. Ryan and E. Diller are with the department of Mechanical and Industrial Engineering, University of Toronto, Toronto, ON, M5S 3G8

Email: ediller@mie.utoronto.ca

and the rotational motion of the magnets can be realized using inexpensive DC or stepper motors. Thus this system is a simple, low-cost option for untethered magnetic control. A schematic image of the proposed system in shown in Fig. 1.

The system we propose is able to achieve or exceed many of the supposed advantages of electromagnetic devices while avoiding the problems normally attributed to permanent magnet systems. For example, the angular positions of the magnets can be set such that the field and field gradient at the position of the microrobot have zero magnitude which is similar to the ability to turn off the field generated by an electromagnetic system. Additionally, the system we are presenting is able to produce rotating fields with frequency on the order of hundreds of hertz which is comparable to the capability of electromagnetic systems. Lastly, the permanent magnets produce a magnetic field without any heat production.

II. Control using Rotatable Permanent Magnets

The untethered micro-device that is to be controlled is assumed to contain a permanent magnet with moment $\vec{m}_d$ and located at position $\vec{p}$. The torque $\vec{T}$ exerted on this magnetic moment when subjected to an applied magnetic field with flux density $\vec{B}(\vec{p})$ at point $\vec{p}$ is given by

$$\vec{T} = \vec{m}_d \times \vec{B}(\vec{p}). \tag{1}$$

This magnetic torque, when unopposed, will orient the magnetic moment in the direction of the applied magnetic field. For device applications in a liquid environment at low rotational speeds, the magnetic moment is able to quickly align with the field. In these cases the magnetic moment can be assumed to be always aligned with the field and therefore the device heading can be controlled simply by adjusting the direction of the applied field.

The rotatable permanent magnets that are used for device actuation (henceforth referred to as actuator magnets) are approximated as point dipole sources located at the volumetric center of the magnets. The error associated with this approximation is less than 2% for cubic magnets located at least two side lengths from the workplace [17]. The magnetic field $\vec{B}$ at point $\vec{p}$ in the workplace is given by the linear addition of the fields from all *N* actuator magnets as

$$\vec{B}(\vec{p}) = \sum_{i=1}^{N} \frac{\mu_0 |\vec{m}_i|}{4\pi |\vec{r}_i|^3} (3\hat{r}_i \hat{r}_i^{\mathsf{T}} - I)\hat{m}_i \tag{2}$$

where $\mu_0 = 4\pi \times 10^{-7}\ \mathrm{Tm \cdot A^{-1}}$ is the permeability of free-space, I is the 3x3 identity matrix, $\vec{r}_i$ is the vector from the center of the i^{th} permanent magnet to position $\vec{p}$, $\hat{r}_i$ is a unit vector in that direction, $\vec{m}_i$ is the magnetic moment of the i^{th} actuator magnet, and $\hat{m}_i$ is a unit vector such that $\vec{m}_i = |\vec{m}_i|\hat{m}_i$.

The actuator magnetic moment unit vector $\hat{m}$ can be parameterized by the rotational position of the magnet θ (henceforth referred to as motor angle) as

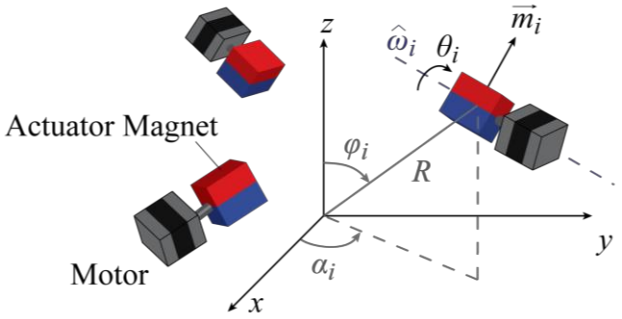

Fig. 1. Schematic image showing three actuator magnets, as well as the magnetic moment $\vec{m}_i$ defined by the motor spin angle θ_i about its rotational axis $\hat{\omega}_i$. The magnet center points are defined using spherical coordinates (R, α_i, φ_i).

$$\hat{m}(\theta) = R_{zy}\begin{bmatrix}\cos(\theta) & \sin(\theta) & 0\end{bmatrix}^{\mathsf{T}} \tag{3}$$

where R_{zy} is a *zy* Euler angle rotation matrix defined by two rotation angles β and ϕ, which correspond to rotations around the *z* and *y* axes, respectively.

The force exerted on the magnetic device with moment $\vec{m}_d$ at location $\vec{p}$ from the applied field produced by the actuator magnets, assuming no current flowing in the workspace, is given by

$$\vec{F}(\vec{p}, \vec{m}_d) = (\vec{m}_d \cdot \nabla)\vec{B}(\vec{p}) \tag{4}$$

$$= \sum_{i=1}^{N} \left\{ \frac{3\mu_0 |\vec{m}_i|}{4\pi |\vec{r}_i|^4} \left(\hat{m}_i \hat{r}_i^{\mathsf{T}} + \hat{r}_i \hat{m}_i^{\mathsf{T}} - \left[5\hat{r}_i \hat{r}_i^{\mathsf{T}} - I \right] (\hat{m}_i \cdot \hat{r}_i) \right) \right\} \vec{m}_d .$$

In order to control a device with 5 actuation DOF, the orientation and position of the device are adjusted by changing the magnetic field and force, respectively. The input to the actuation system is the motor angles of all the actuator magnets $\vec{\theta} = \{\theta_1 \ldots \theta_N\}^{\mathsf{T}}$. That is because the field and force that is produced at the microrobot is a function of the magnetic moment $\vec{m}_i$ of each actuator magnet, which in turn is a function of the rotation of the magnets $\vec{\theta}$. Due to the non-linear relationship between the control input and the outputs, linear algebra techniques cannot be used to determine the required inputs as they can be with most electromagnet systems. Thus, we consider the control inputs to be a solution to the optimization problem

$$\min f = K\left\| \vec{B}(\vec{\theta}) - \vec{B}_0 \right\|^2 + (1-K)\left\| \vec{F}(\vec{\theta}) - \vec{F}_0 \right\|^2 \tag{5}$$

where $\vec{B}_0$ and $\vec{F}_0$ are the desired field and force outputs, respectively; $\vec{B}(\vec{\theta})$ and $\vec{F}(\vec{\theta})$ are the field and force vectors that are produced for a given set of motor angles , respectively; and K is used to weigh the two halves of the equation to account for the difference in the units of measurement for the field and force, where $0 < K < 1$.

For an arbitrary permanent magnet configuration and arbitrary desired field and force vectors $\vec{B}_0$ and $\vec{F}_0$, this

optimization problem is non-convex with greater than zero local minima. The optimization is thus performed using a gradient descent method with multiple starting points in order to improve the likelihood of finding the global minimum. For use in a feedback controller, control outputs are needed quickly in order to ensure control over the device is not lost and therefore in general there will be insufficient time to ensure that the global minimum of (5) has been found. Instead, the search is ended when an acceptable field and force have been found. The acceptability of the results is determined by comparing the magnitude and angle error between both $\vec{B}(\vec{\theta})$ and $\vec{B}_0$ as well as $\vec{F}(\vec{\theta})$ and $\vec{F}_0$ to a user-controlled threshold error value (in practice, several percent of the full magnitude and within a few degrees).

A further consideration for feedback control is that the field and force applied to the device will fluctuate as the magnets are rotated from one set of motor angles to the next. For systems using motors with limited speed, this phenomena can have a large effect on the position and orientation of the device during these transitions. To minimize this effect, a $\| \Delta\vec{\theta} \|^2$ term could be added to (5), with the purpose of reducing the change in motor angles relative to the previous set of angles at each instance of the control update.

III. Design of Permanent Magnet Configuration

A. General Considerations

Once the controller has been defined, it can be used to quantify the performance of a given fixed configuration of actuator magnets, as defined by the position and rotation axis of each magnet in 3D space. The goal in designing an effective actuation system is to determine an actuator magnet configuration that is able to generate fields and forces with sufficiently large magnitudes isotopically across the operating workspace. To determine the capability of a given magnet arrangement the maximum field and force magnitude that can be generated in a number of directions is calculated. In this work, the maximum field is found in 13 candidate directions and the maximum force is found in 13 directions for each of 13 device orientations, resulting in 169 total force measurements. These maximum values are denoted $\vec{B}_{\max}$ and $\vec{F}_{\max}$, respectively. The strength and isotropy of the field and force production capabilities of the system are then quantified using four terms corresponding to the average force and field strength and one minus the normalized standard deviation of the force and field strengths as

$$B_{str} = \mathrm{AVG}\left(\vec{B}_{\max}\right), \qquad F_{str} = \mathrm{AVG}\left(\vec{F}_{\max}\right)$$

$$B_{iso} = 1 - \frac{\mathrm{SD}(\vec{B}_{\max})}{B_{str}}, \text{ and } \quad F_{iso} = 1 - \frac{\mathrm{SD}(\vec{F}_{\max})}{F_{str}}, \tag{6}$$

where for a vector v, AVG(v) and SD(v) denote the mean and standard deviation of v, respectively. The overall system performance is a weighted sum Q of these four metrics as

$$Q = K_1 B_{str} + K_2 B_{iso} + K_3 F_{str} + K_4 F_{iso}. \tag{7}$$

The system parameters that can be modified in order to affect the overall performance are the positions of the centers of the actuator magnets, the rotational axes of the magnets, the number of magnets, and the magnitude of the dipole moments of the magnets, which is proportional to the magnet volume. The formulation of the optimization given in (6) and (7) could also be adapted to improve other criteria such as workspace size.

The position of each actuator magnet is defined using three parameters (i.e. an x, y, and z coordinate) while the axis of rotation can be expressed using two coordinates. The magnitude of the field produced from a single actuator magnet decreases proportionally to the cube of the distance between the magnet and the workspace, while the magnitude of the gradient decreases proportionally to the distance raised to the fourth power. Therefore, in order to generate the strongest possible fields and gradients, each magnet should be positioned as close to the workspace as possible, subject to workspace constraints, and ensuring sufficient separation to justify the dipole magnet approximation. If all the magnets lie the same distance R from the workspace, the i^{th} magnet position can be defined using spherical coordinates (R, α_i, φ_i) where α_i is the azimuth angle and φ_i is the inclination angle as shown in Fig. 1. The rotational axis of the i^{th} magnet, of unit magnitude, can also be defined using two spherical coordinate parameters which are equivalent to the z and y Euler angle rotations mentioned above in (3).

B. Prototype System

For the prototype system proposed in this paper, cubic magnets with dipole moment $|\vec{m}_i| = 16.6$ Am^2 were positioned at a distance of R = 7.5 cm from the center of the workspace. This combination of magnet strength and workspace distance was chosen because magnetic fields and gradients of sufficient strength can be generated, and the error associated with the dipole approximation for cubic magnets is less than 0.5 % [17]. Other constraints for the prototype are that the magnets and motors be placed without physically interfering, and that the maximum magnetic torque between actuator magnets can be overcome by each motor.

Once the magnet dipole magnitude and workspace separation were decided, the configuration for the prototype system, capable of a high level of control, was found by modifying the spherical positions and rotational axes of the magnets in order to maximize the Q metric defined above in (7). For this optimization, the controlled device was assumed to have a magnetic moment of 10^{-6} Am^2. This optimization was performed manually for the cases of both six and eight actuator magnets, with results shown in Table I. Due to the large search space ($4N$ positioning parameters) this system optimization process is done manually for the prototype. The results obtained indicate that the prototype is "good enough" to achieve feedback control of a micro-scale magnetic device. However, a more rigorous optimization of the design using the fitness function (7) would result in a higher-performing system, especially in cases with more complex application

TABLE I. PERFORMANCE COMPARISON FOR PROTOTYPE SIX- AND EIGHT-MAGNET SYSTEMS

Number of actuator magnets	B_{str} (mT)	B_{iso} (%)	F_{str} (μN)	F_{iso} (%)
6	24.7	84.7	0.671	75.8
8	30.1	92.8	0.936	84.2

TABLE II: POSITIONS AND ROTATIONAL AXES DEFINED IN SPHERICAL COORDINATES FOR THE EIGHT ACTUATOR MAGNETS IN THE PROTOTYPE SYSTEM

Magnet	Positions (deg)		Rotational axes (deg)	
	α_i	φ_i	β_i	ϕ_i
1	335	115	70	60
2	40	105	225	145
3	235	112	315	20
4	90	45	148	235
5	198	45	265	260
6	305	55	25	225
7	70	180	275	90
8	166	115	350	130

constraints such as a system built into an inverted microscope or for medical applications.

The results presented in Table 1 suggests that an eight magnet system is able to produce both stronger and more isotropic fields and forces relative to a six magnet system. This is a similar observation to that seen in the design of electromagnet devices [1]. Another advantage to using more actuator magnets is that the size of the solution set for a particular desired field and force is increased, i.e. a field and force can be generated using a larger number of different actuator motor angles. This additional solution space makes it easier to minimize the change in motor angles between control updates. For these reasons, the prototype was constructed using eight permanent magnets in the state analyzed in Table I, and the exact positions and rotational axes of each magnet are presented in Table II. A photo of the prototype is shown in Fig. 2.

For a 7 mm diameter spherical workspace, the field and force gradient are uniform within 10% of the nominal value. For applications requiring a larger workspace the position of the micro-device must be tracked in order to determine the field and force at the correct location. Magnetic interaction between actuator magnets also affects the performance of the system. Large magnetic torques due to closely positioned actuator magnets increase the frequency of motor skipping and necessitate running the motors at a fraction of their top speed. The maximum magnetic torque that any of the actuator magnets will experience in this configuration is 0.29 Nm.

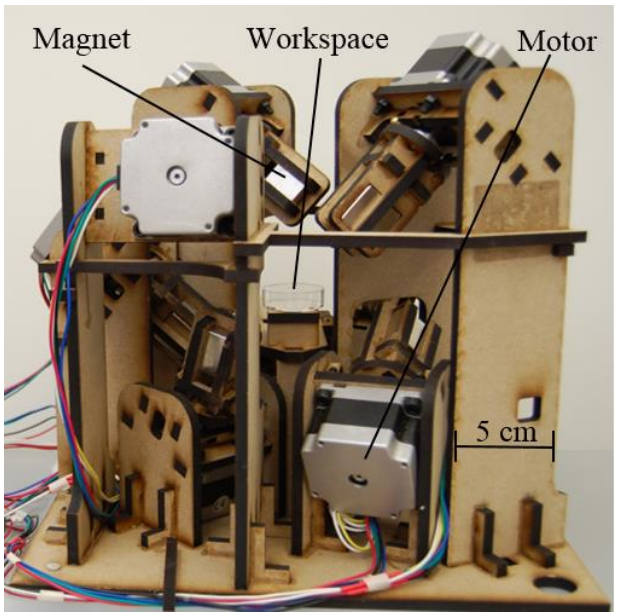

Fig. 2. Side-view of the rotating magnet prototype system. Video of the prototype during operation is available in the supplementary materials.

The permanent actuator magnets used for the prototype system are transversely magnetized, grade N42 cubic NdFeB magnets with side length equal to 2.54 cm. Stepper motors of size NEMA 23 and capable of 0.39 Nm of stall torque were used to rotate the magnets at speeds up to 120 RPM. These motors have average capabilities and a future version of the control system could be improved through the use of motors with higher torque and rotational speeds. The stepper motors are controlled using motor driver boards (Quadstepper Motor Driver Board, SparkFun). Motor position feedback is obtained using magnetic rotary encoders (AS5040, ams AG). The driver boards and encoders were interfaced using a digital I/O board (USBDIO-48, Accessio) to a PC running Ubuntu Linux with custom control code.

The structural pieces of the prototype were assembled using laser-cut pieces of high-density fiberboard. Two stationary cameras (FO134TC, Foculus) provide feedback from the top and side of the prototype. For feedback control, a microrobot detection algorithm was implemented using a threshold function and Hough Transform using the openCV library, capable of detection at up to 60 fps. The total cost of the prototype (magnets, motors, motor drivers, encoders and structural elements) is approximately 1000 USD. Additional components such as PC, data acquisition card and cameras cost about 2000 USD.

IV. RESULTS

A. System Characterization

To demonstrate the capability of the prototype system, we test the static fields it can generate, and perform several proof-of-concept force-application experiments including a feedback-controlled motion experiment.

The static field generation capability of the system is shown by requesting a 30 mT field in eight directions as well as a

TABLE III: COMPARISON OF THE MEASURED FIELD TO THE 30MT DESIRED FIELD IN NINE DIFFERENT DIRECTIONS

Test	1	2	3	4	5	6	7	8	9
$B_{desired}$ (mT)	$\begin{bmatrix}0.00\\0.00\\0.00\end{bmatrix}$	$\begin{bmatrix}30.00\\0.00\\0.00\end{bmatrix}$	$\begin{bmatrix}0.00\\-30.00\\0.00\end{bmatrix}$	$\begin{bmatrix}0.00\\0.00\\30.00\end{bmatrix}$	$\begin{bmatrix}-21.2\\21.2\\0.00\end{bmatrix}$	$\begin{bmatrix}21.21\\0.00\\-21.21\end{bmatrix}$	$\begin{bmatrix}0.00\\21.21\\21.21\end{bmatrix}$	$\begin{bmatrix}-17.32\\-17.32\\-17.32\end{bmatrix}$	$\begin{bmatrix}17.32\\-17.32\\17.32\end{bmatrix}$
$B_{measured}$ (mT)	$\begin{bmatrix}0.13\\-0.38\\0.28\end{bmatrix}$	$\begin{bmatrix}30.38\\-0.44\\-0.76\end{bmatrix}$	$\begin{bmatrix}-1.77\\-30.42\\0.16\end{bmatrix}$	$\begin{bmatrix}-0.95\\-0.01\\30.09\end{bmatrix}$	$\begin{bmatrix}-21.09\\20.29\\0.35\end{bmatrix}$	$\begin{bmatrix}22.68\\0.68\\-21.79\end{bmatrix}$	$\begin{bmatrix}0.46\\21.45\\22.09\end{bmatrix}$	$\begin{bmatrix}-17.94\\-17.59\\-18.00\end{bmatrix}$	$\begin{bmatrix}16.27\\-17.21\\17.31\end{bmatrix}$
$\frac{\lvert B_{dipole} \rvert}{\lvert B_{measured} \rvert}$	-	0.987	0.985	0.997	1.025	0.954	0.974	0.971	1.023
$\angle$ (deg)	-	1.65	3.35	1.81	1.30	1.69	1.20	0.59	1.60

field of zero magnitude and comparing this desired field to the field produced by the system at the center of the workspace, measured using a single-axis gaussmeter (model 425, Lakeshore) in the *x, y,* and *z* directions. Table III shows the desired field, the average measured field for two trials, the magnitude ratio of desired field to measured field, and the angle between the desired and measured field. The misalignment and magnitude difference between the desired field and measured field is small, less than 3.35° and 4.6%, respectively. These errors are likely due to fabrication and position errors in the laser-cut prototype frame. For increased accuracy, a calibration procedure to find the actual magnet positions and rotation axes can reduce these errors in future systems.

The static force production capability of the system is characterized by measuring the heading of a small magnetic device as the device is subjected to a desired force. The device used for this test is a N50 cubic NdFeB magnet with side length equal to 250 µm and the test is conducted in a horizontal container filled with silicone oil with a viscosity of 350 cSt. The micromagnet is maneuvered away from the wall of the workspace and then held stationary by applying a zero force. Once stationary, a set of motor angles is found that result in a desired force direction and magnitude. After the motors have completed the rotation to the set of motor angles, the heading of the micromagnet over time is measured and compared to the requested force direction. Three different force directions were tested (*x, y,* and *xy*) and the heading error averaged over five trials per heading direction was found to be 4.6°, 5.2°, and 5.3°, respectively. The speed of the micromagnet during each experiment varies between trials, an effect likely due to changing friction and viscous drag from dragging the magnet along the bottom of the container.

B. Proof-of-Concept Feedback Control Experiments

To demonstrate the full capabilities of the prototype, a proof-of-concept 2D feedback control experiment was conducted in a horizontal and vertical plane. Using the same micromagnet and fluid environment from the previous test, the task was to pull the micromagnet using the magnetic force to three sequential goal points in the shape of a triangle. The 2D location of the micromagnet was obtained from the top-view camera at a rate of 60 Hz. At every occurrence of a control update, the requested magnetic force is directed such that the robot travels towards the next goal point as well as back to the path. By limiting the change in the desired force vector between control updates, the required change in motor angles is reduced. In practice this is implemented when a goal point is reached by reducing the magnetic force at the robot's location to zero then increasing the force from zero in the direction of the next goal point. The requested field is held constant in magnitude (10 mT) and direction but is allowed to vary up to 8 mT and 12° in order to increase the speed of finding a suitable solution to (5) in the shortest amount of time. Using our simple gradient-descent search algorithm, the computation time for one control update can be completed on average in 0.001 s. The algorithm explained above was used for the vertical experiments except that a constant, vertical, magnetic force offset was applied to counteract gravity.

Five trials of the control experiment were completed in both the horizontal and vertical planes. The average deviation across the horizontal trials was 39 µm and the average velocity 173 µm·s^{-1}. The average deviation across the vertical trials was 56 µm and the average velocity 174 µm·s^{-1}. Results of a typical horizontal feedback control test are shown in Fig. 3. The average deviation for this single trial is 43 µm. Similar to the force heading experiments, the velocity of the micromagnet is not consistent because of changing friction and viscous drag.

V. CONCLUSIONS

We have shown the capability for a simple permanent-magnet actuation system to achieve an equivalent level of control to electromagnetic systems for the motion of untethered micro-scale magnetic devices. The prototype system introduced here is capable of producing fields of 30 mT and field gradients of 0.9 T·m^{-1} in any direction using an inexpensive setup. Feedback control of a micro sized device has been demonstrated in both the horizontal and vertical planes with average deviations of 39 µm and 56 µm, respectively. These results compare favorably with existing electromagnet control systems, all without the use of heat-generating coils close to the workspace and with no hazardous

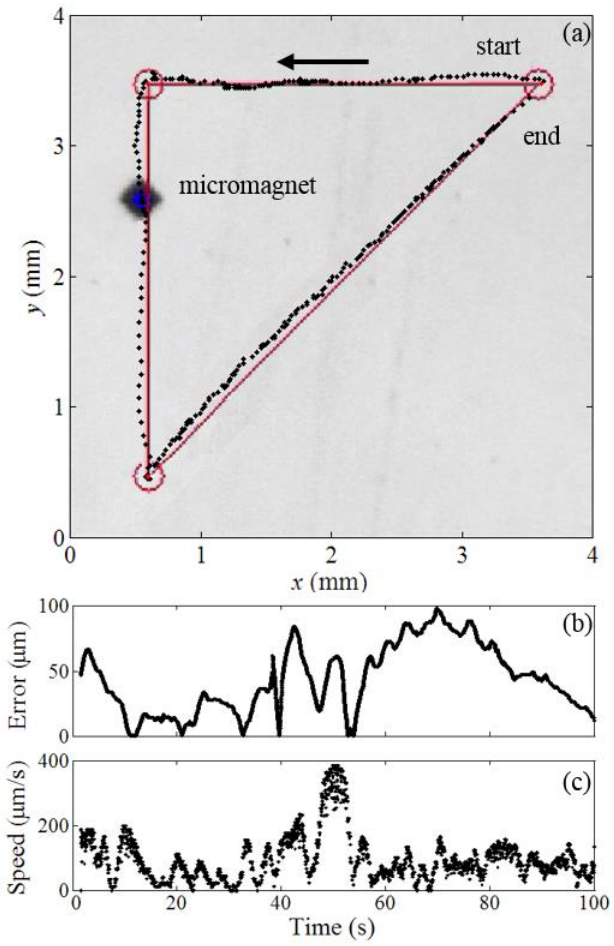

Fig. 3. A typical feedback result for a 250µm magnet performing path following in the horizontal plane. (a) Path of the micromagnet in black and the goal points and desired path in red. The micromagnet deviation from the path (b) and speed (c).

translating magnets as used in previous permanent magnet control systems. Lastly we present a basic system design optimization that can be adapted for any given application requirement.

Although the prototype system presented here contains motors that generate heat and are positioned close to the workspace, this was done for ease of construction and is not inherent to the overall control method that we are proposing. Future versions could have motors placed an arbitrary distance away from the actuator magnets in order to limit the heat that is transferred to the workspace. Vibrations generated by the motors were imperceptible using the feedback system but could be further reduced though the use of vibration damping mounts.

REFERENCES

[1] M. P. Kummer, J. J. Abbott, B. E. Kratochvil, R. Borer, A. Sengul, and B. J. Nelson, "Octomag: An electromagnetic system for 5-DOF wireless micromanipulation," *IEEE Trans. on Robotics*, vol. 26, no. 6, pp. 1006–1017, 2010.

[2] F. Carpi and C. Pappone, "Stereotaxis niobe magnetic navigation system for endocardial catheter ablation and gastrointestinal capsule endoscopy," *Ex. Review of Med. Dev.*, vol. 6, no. 5, pp. 487–498, 2009.

[3] A. W. Mahoney and J. J. Abbott, "5-DOF manipulation of an untethered magnetic device in fluid using a single permanent magnet," *Proc. of Robotics: Science and Systems*, Berkeley, USA, July 2014.

[4] M. S. Sakar, E. B. Steager, A. Cowley, V. Kumar, and G. J. Pappas, "Wireless manipulation of single cells using magnetic microtransporters," *IEEE Int. Conf. on Robotics and Automation*, 2011, pp. 2668–2673.

[5] J. D. Keuning, J. de Vriesy, L. Abelmanny, and S. Misra, "Image-based magnetic control of paramagnetic microparticles in water," *IEEE Int. Conf. on Intelligent Robots and Systems*, 2011, pp. 421–426.

[6] H. Keller, A. Juloski, H. Kawano, M. Bechtold, A. Kimura, H. Takizawa, and R. Kuth, "Method for navigation and control of a magnetically guided capsule endoscope in the human stomach," *IEEE Int. Conf. on Biomedical Robotics and Biomechatronics.*, 2012, pp. 859–865.

[7] E. Diller, J. Giltinan, and M. Sitti, "Independent control of multiple magnetic microrobots in three dimensions," *The Int. J. of Robotics Research*, vol. 32, no. 5, pp. 614–631, 2013.

[8] S. Erni, S. Schürle, A. Fakhraee, B. E. Kratochvil, and B. J. Nelson, "Comparison, optimization, and limitations of magnetic manipulation systems," *J. of Micro-Bio Robotics*, vol. 8, no. 3-4, pp. 107–120, 2013.

[9] D. R. Frutiger, K. Vollmers, B. E. Kratochvil, and B. J. Nelson, "Small, fast, and under control: wireless resonant magnetic micro-agents," *The Int. J. of Robotics Research*, vol. 29, no. 5, pp. 613–636, 2010.

[10] C. Pawashe, S. Floyd, and M. Sitti, "Modeling and experimental characterization of an untethered magnetic micro-robot," *The Int. J. of Robotics Research*, vol. 28, no. 8, pp. 1077–1094, 2009.

[11] T. W. Fountain, P. V. Kailat, and J. J. Abbott, "Wireless control of magnetic helical microrobots using a rotating-permanent-magnet manipulator," *IEEE Int. Conf. on Robotics and Automation*, 2010, pp. 576–581.

[12] A. W. Mahoney and J. J. Abbott, "Generating rotating magnetic fields with a single permanent magnet for propulsion of untethered magnetic devices in a lumen," *IEEE Trans. on Robotics*, vol. 30, no. 2, pp. 411–420, 2014.

[13] G. Lien, C. Liu, J. Jiang, C. Chuang, and M.-T. Teng, "Magnetic control system targeted for capsule endoscopic operations in the stomach—design, fabrication, and in vitro and ex vivo evaluations," *IEEE Trans. on Biomedical Engineering*, vol. 59, no. 7, pp. 2068–2079, 2012.

[14] S. Yim and M. Sitti, "Design and rolling locomotion of a magnetically actuated soft capsule endoscope," *IEEE Trans. on Robotics*, vol. 28, no. 1, pp. 183–194, 2012.

[15] G. Ciuti, P. Valdastri, A. Menciassi, and P. Dario, "Robotic magnetic steering and locomotion of capsule endoscope for diagnostic and surgical endoluminal procedures," *Robotica*, vol. 28, no. 2, pp. 199–207, 2010.

[16] W. Zhang, Y. Meng, and P. Huang, "A novel method of arraying permanent magnets circumferentially to generate a rotation magnetic field," *IEEE Trans. on Magnetics*, vol. 44, no. 10, pp. 2367–2372, 2008.

[17] A. J. Petruska and J. J. Abbott, "Optimal permanent-magnet geometries for dipole field approximation," *IEEE Trans. on Magnetics*, vol. 49, no. 2, pp. 811–819, 2013.